Spin dynamics of half-doped $La_{3/2}Sr_{1/2}NiO_4$

P. G. Freeman,* A. T. Boothroyd, and D. Prabhakaran
Department of Physics, Oxford University, Oxford, OX1 3PU, United Kingdom

C. D. Frost
ISIS Facility, Rutherford Appleton Laboratory, Chilton, Didcot, OX11 0QX, United Kingdom

M. Enderle and A. Hiess
Institut Laue-Langevin, BP 156, 38042 Grenoble Cedex 9, France
(Received 4 October 2004; published 18 May 2005)

We report polarized- and unpolarized-neutron inelastic-scattering measurements of the magnetic excitation spectrum in the spin-charge ordered phase of $La_{3/2}Sr_{1/2}NiO_4$. Up to energies of $\sim$30 meV we observe broad magnetic modes characteristic of a near checkerboard ordering. A linear spin-wave model for an ideal checkerboard ordering with a single antiferromagnetic exchange interaction $J'=5.8\pm0.5$ meV between next-nearest-neighbor spins on Ni^{2+} sites, together with a small *XY*-like single-ion anisotropy, provides a reasonable description of the measured dispersion. Above 30 meV the excitations are not fully consistent with the linear spin-wave model, with modes near the two-dimensional reciprocal space wave vector (0.5, 0.5) having an anomalously large intensity. Furthermore, two additional dispersive modes not predicted by spin-wave theory were observed, both of which are probably magnetic. One disperses away from (0.5, 0.5) in the energy range between 50–56 meV, and the other appears around (h,k) type positions (h,k=integer) in the energy range 31–39 meV. We propose a model in which these anomalous features are explained by the existence of discommensurations in the checkerboard ordering. At low energies there is additional diffuse scattering centred on the magnetic ordering wave vector. We associate this diffuse scattering with dynamic antiferromagnetic correlations between spins attached to the doped holes.

DOI: 10.1103/PhysRevB.71.174412 PACS number(s): 71.45.Lr, 75.40.Gb, 75.30.Et, 75.30.Fv

I. INTRODUCTION

The existence of charge-ordering phenomena continues to attract considerable interest, especially concerning the properties of layered transition-metal oxides. The nature of the charge ordering in these materials depends on the degree of doping relative to a Mott insulating phase. At low doping the charges tend to segregate into parallel lines. The resulting stripe superstructures have been widely discussed in connection with high-temperature superconductivity in cuprates.[1] At higher doping there is a competition between charge-ordered and metallic states. The existence of magnetic correlations is also an important factor, and the coupling between charge, orbital, spin, and lattice degrees of freedom can often stabilize novel ordered states.

At half doping, systems with dominant Coulomb repulsions are expected to exhibit a stable Wigner crystal state, which in the case of a two-dimensional square lattice takes the particularly simple form of a checkerboard pattern. This type of charge order has been observed in the isostructural layered perovskites $La_{3/2}Sr_{1/2}NiO_4$,[2] $La_{1/2}Sr_{3/2}MnO_4$,[3] and $La_{3/2}Sr_{1/2}CoO_4$.[4] Interestingly, checkerboard charge order has also recently been observed at doping levels well below 0.5 in $Bi_2Sr_2CaCu_2O_{8+\delta}$ (Ref. 5) and $Ca_{2-x}Na_xCuO_2Cl_2$,[6] with a periodicity of four Cu atoms. Further experimental studies of simple systems with checkerboard charge order could help explain the formation of electronically ordered states in more complex systems.

In this paper we describe a neutron-inelastic-scattering study of the spin excitations in the half-doped layered nickelate $La_{3/2}Sr_{1/2}NiO_4$. This compound exhibits checkerboard charge order below $T_{CO}\approx480$ K.[2,7] Below $T_{IC}\approx180$ K the checkerboard pattern becomes slightly incommensurate, and below $T_{SO}\approx80$ K it is accompanied by incommensurate magnetic order.[7] A spin-reorientation transition has been observed at $T_{SR}=57$ K.[8] By mapping out the spin-excitation spectrum of $La_{3/2}Sr_{1/2}NiO_4$ as a function of energy and wave vector and comparing the dynamic response with that of other charge-ordered compounds we hope to gain a better understanding of the interactions that stabilize the ground state in these systems.

Previously, the spin-excitation spectrum of $La_{2-x}Sr_xNiO_4$ has been investigated over a wide range of wave vector and energy in stripe-ordered compounds with $x=0.275$,[9] $x=0.31$,[10] and $x=1/3$.[11,12] The spin excitations are highly two dimensional (2D), and fairly independent of x over this small range of compositions studied. Over most of the energy range the magnetic dynamics can be described in terms of spin-wave excitations of the antiferromagnetically ordered Ni spins in the region between the charge stripes.[11] At low energies, however, a second magnetic component is observed that has been shown to come from quasi-1D antiferromagnetic spin fluctuations along the stripes themselves.[12]

Figure 1 illustrates how the different ordered phases in $La_{3/2}Sr_{1/2}NiO_4$ can be identified in diffraction measurements. Figure 1(a) is a simplified model of the ground-state spin-charge order within the NiO_2 layers of $La_{3/2}Sr_{1/2}NiO_4$ neglecting the small incommensurate modulation. For present purposes we assume the doped holes are site centered, so that

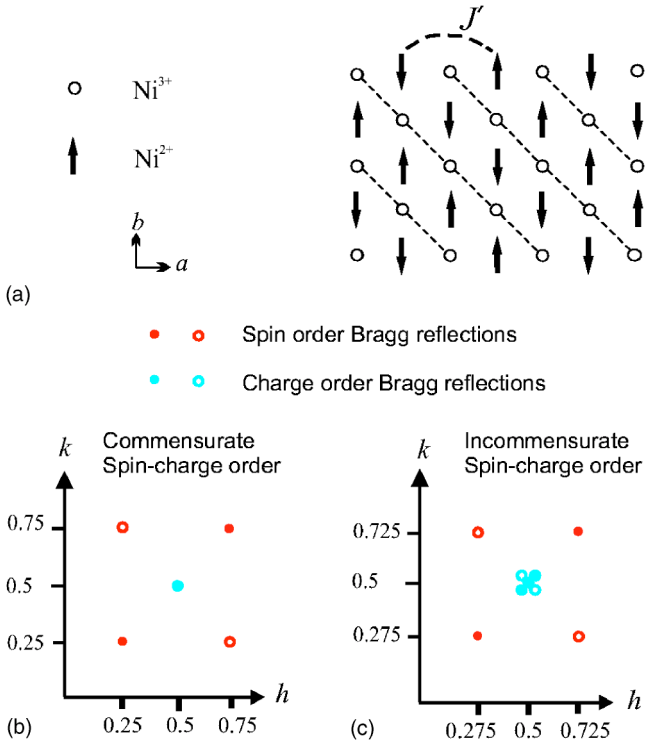

FIG. 1. (Color online) (a) Ideal checkerboard spin-charge ordering in a NiO_2 square lattice. Circles represent Ni^{3+} holes and solid arrows represent spins on Ni^{2+} sites. The broken lines are included to highlight that the spin pattern breaks the 2D symmetry of the checkerboard charge ordering. J' is the exchange coupling parameter of the Ni^{2+} spins across the Ni^{3+} site. This commensurate ordering is not realized in practice in $La_{3/2}Sr_{1/2}NiO_4$. (b) Diagram of part of the (h,k) plane in 2D reciprocal space showing the positions of the first-order magnetic and charge order Bragg peaks for the ideal checkerboard ordering represented in (a). The peaks from the equivalent domain in which the magnetic ordering is rotated by 90° relative to that in (a) are superimposed. (c) The same diagram as (b) except with the magnetic and charge order Bragg peaks observed in the incommensurate ordered phase of $La_{3/2}Sr_{1/2}NiO_4$. For simplicity we neglect the variation in the peak positions in the direction perpendicular to the NiO_2 plane.

the checkerboard pattern is derived from alternating Ni^{2+} and Ni^{3+} ions carrying spins $S=1$ and $S=\frac{1}{2}$, respectively. The $S=1$ spins are assumed to be ordered antiferromagnetically, but we make no assumption at this stage about magnetic order of the $S=\frac{1}{2}$ spins (this issue will be addressed later in the paper). The positions in reciprocal space of the corresponding Bragg peaks are shown in Fig. 1(b). Peaks from the charge order have two-dimensional wave vectors (in units of $2\pi/a$) $(h+\frac{1}{2},k+\frac{1}{2})$, where h and k are integers.[14] The magnetic order has double the periodicity of the charge order, so peaks from the magnetic order appear at $(h+\frac{1}{2},k+\frac{1}{2})\pm(\frac{1}{4},\frac{1}{4})$. Rotation of the ordering pattern by 90° generates an equivalent magnetic structure, this time with magnetic peaks at $(h+\frac{1}{2},k+\frac{1}{2})\pm(\frac{1}{4},-\frac{1}{4})$. In the absence of a symmetry-breaking interaction we expect an equal population of these two domains, so the pattern of Bragg peaks will be a superposition, as shown in Fig. 1(b).

The actual spin-charge-ordered phase of $La_{3/2}Sr_{1/2}NiO_4$ observed below T_{IC} does not conform to the ideal structure shown in Fig. 1(a). Instead, the magnetic Bragg peaks are found at the incommensurate positions $(h+\frac{1}{2},k+\frac{1}{2},l)\pm(\epsilon/2,\epsilon/2,0)$ with l an odd integer and $(h+\frac{1}{2},k+\frac{1}{2},l)\pm(\epsilon/2,-\epsilon/2,0)$ with l an even integer, where $\epsilon\approx0.44$. [7,8,13] New charge-order satellite peaks appear at $(h\pm\epsilon,k\pm\epsilon)$ in addition to the checkerboard charge-order peak at $(h+\frac{1}{2},k+\frac{1}{2})$, with little or no l dependence.[7,8] The full set of 2D magnetic and charge-order wave vectors for the incommensurate phase of $La_{3/2}Sr_{1/2}NiO_4$, including those for the 90° domain, is shown in Fig. 1(c).

Kajimoto *et al.*[7] suggested that two types of charge order coexist in the incommensurate phase, one part of the system being charge ordered in a checkerboard pattern and the other part adopting an incommensurate, stripelike, spin-charge order. These authors developed models for the latter component based on the introduction of diagonal discommensurations in the ideal checkerboard spin-charge structure of Fig. 1(a). As pointed out by Kajimoto *et al.*, the stability of the incommensurate structure is probably the result of a competition between magnetic and electrostatic energy. The strong superexchange interaction favors having antiparallel spins on nearest-neighbor Ni sites, whereas the Coulomb interaction tries to have a uniform charge density.

II. EXPERIMENTAL DETAILS

The neutron-scattering measurements were performed on a single crystal of $La_{3/2}Sr_{1/2}NiO_4$ grown by the floating-zone method.[15] The crystal was a cylinder 35 mm in length and 7 mm in diameter. The oxygen content of the crystal was determined by thermogravimetric analysis (TGA) to be 4.02 ± 0.01. This is the same crystal that was used in our earlier neutron-diffraction and magnetization study of the magnetic order.[8]

The majority of the unpolarized-neutron-scattering measurements were performed on the time-of-flight chopper spectrometer MAPS at the ISIS Facility. The crystal was mounted on MAPS in a closed-cycle refrigerator and aligned with the c axis parallel to the incident beam direction. A Fermi chopper was used to select the incident neutron energy. Incident energies of 60 and 100 meV were used. The intensity was normalized and converted to units of scattering cross section (mb sr^{-1} meV^{-1} [f.u.]$^{-1}$) by comparison with measurements from a standard vanadium sample. Scattered neutrons were recorded in large banks of position-sensitive detectors. The spin dispersion was found to be highly two dimensional. Hence, we analyzed the data by making a series of constant energy slices and projecting the intensities onto the (h,k) two-dimensional reciprocal lattice plane.

Further unpolarized- and polarized-neutron measurements were performed on the triple-axis spectrometers IN8 and IN20 at the Institut Laue-Langevin. The energies of the incident and scattered neutrons were selected by Bragg reflection from a double-focusing bent Si crystal monochromator on

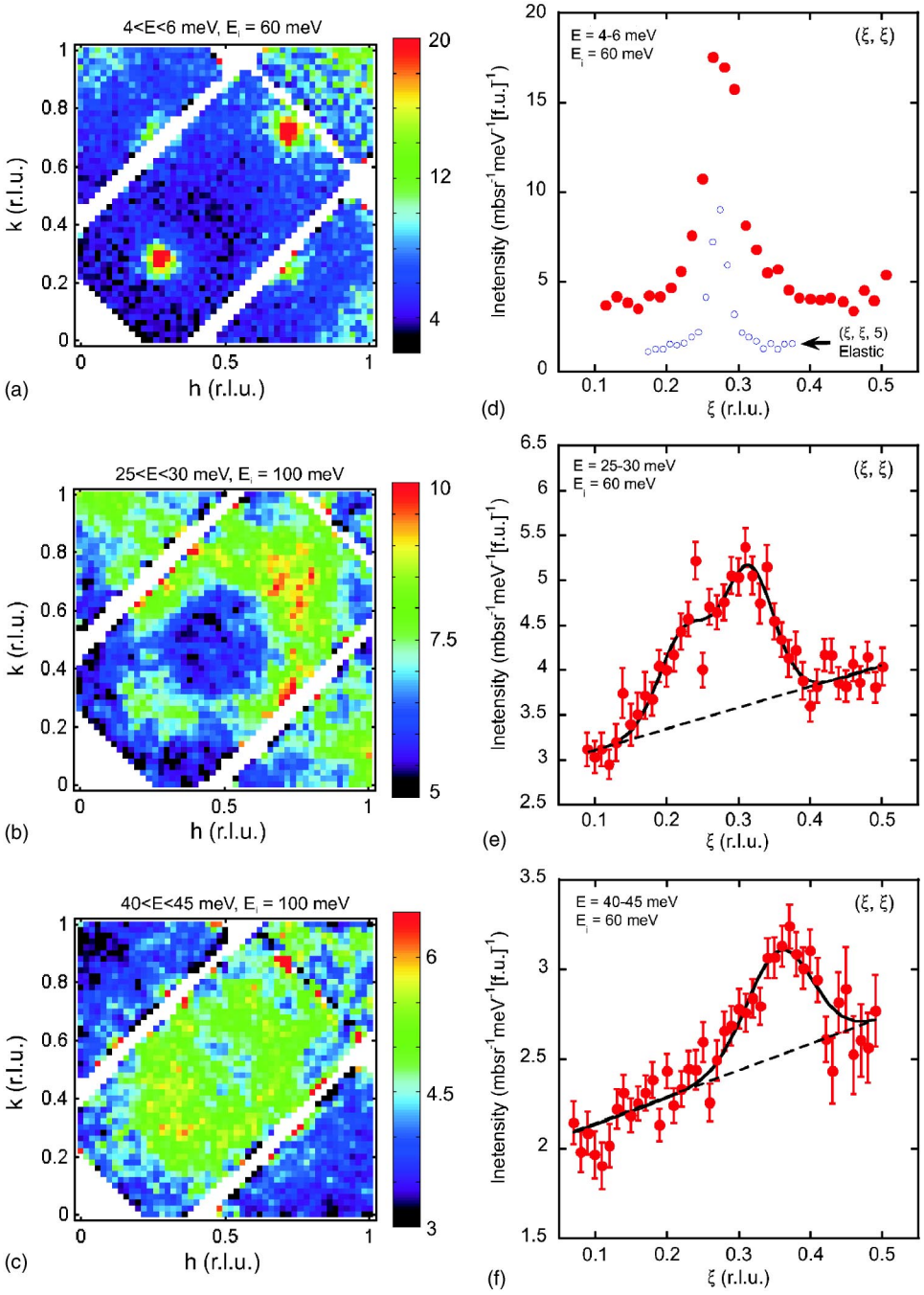

FIG. 2. (Color online) Neutron-scattering measurements from $La_{3/2}Sr_{1/2}NiO_4$ measured on MAPS at $T=10$ K. (a)–(c) are constant-energy slices showing the variation of the intensity in the (h,k) plane at different energies. The data are averaged over the range of energies indicated above the figures. The incident neutron energy was 60 meV for (a) and 100 meV for (b) and (c). Data from four equivalent Brillouin zones have been averaged. (d)–(f) show cuts along the (ξ,ξ) direction for the same energies as shown in (a)–(c). The solid lines are the results of fits with one Gaussian [(d) and (f)] or two Gaussians [(e)] on a linear background. In (d) we also display the (0.275, 0.275, 5) magnetic order Bragg peak measured on IN20. The out-of-plane wave vectors for the position (0.275, 0.275) are as follows: (a) and (d) $l=0.55$, (b) $l=2.3$, (e) $l=3.0$, (c) $l=3.45$, and (f) $l=5.2$.

IN8, and an array of Heusler alloy crystals on IN20. On both instruments the data were obtained with a final neutron wave vector of 2.66 $Å^{-1}$, and a pyrolytic graphite (PG) filter was placed between the sample and analyzer to suppress higher-order harmonic scattering. For polarized-neutron scattering on IN20 the spin polarization **P** was maintained in a specified orientation with respect to the neutron wave vector **Q** by an adjustable guide field of a few mT at the sample position. For the experiment on IN8 the crystal was orientated with the [100] and [010] crystal directions in the horizontal scattering plane, so that $(h,k,0)$ positions in reciprocal space could be accessed. On IN20, we mounted the crystal with the [001] and [110] directions in the horizontal scattering plane, so that (h,h,l) positions in reciprocal space could be accessed.

III. RESULTS

Figures 2(a)–2(c) show constant-energy slices from runs performed at $T=10$ K on MAPS.[16] The slices have been averaged over a range of energies, as indicated in the figures. In (a), the range is 4–6 meV, and the intensity is seen to be enhanced at the four equivalent magnetic order wave vectors $(0.5,0.5)\pm(\epsilon/2,\epsilon/2)$ and $(0.5,0.5)\pm(\epsilon/2,-\epsilon/2)$, where $\epsilon \approx 0.44$. This signal, therefore, corresponds to low-energy spin excitations from the magnetically ordered ground state.

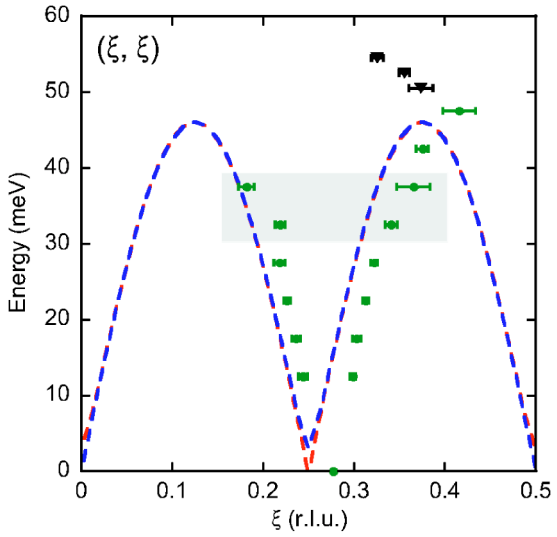

FIG. 3. (Color online) Dispersion of the magnetic excitations in $La_{3/2}Sr_{1/2}NiO_4$ parallel to the (ξ,ξ) direction. The points are the results of fits to cuts such as those shown in Fig. 2. The broken lines are calculated from Eq. (2), the spin-wave dispersion for a checkerboard ordered system with exchange parameter $J'=5.8$ meV and out-of-plane anisotropy $K_c=0.05$ meV. The two branches of the dispersion curve are separated at low energies by a small anisotropy gap which can clearly be seen in Fig. 6(b). Triangles above the calculated dispersion curve indicate the positions of an additional observed scattering mode. The shaded area represents the region in which additional scattering hampers the study of the spin-wave excitations, see Fig. 5.

As the energy increases, the intensity spreads out but initially remains centred on the magnetic wave vectors. This can be seen in Fig. 2(b), which shows data averaged over 25–30 meV. At still higher energies the four blobs of intensity tend to merge towards (0.5, 0.5). This is illustrated in (c), which corresponds to an energy range 40–45 meV.

In Figs. 2(d)–2(f) we plot cuts through the data in the (ξ,ξ) direction for the same energy ranges as used in Figs. 2(a)–2(c). At low energies, $E=4-6$ meV, the scattering takes the form of a single peak centred on the magnetic wave vector. The fitted Gaussian width of this peak converts to a correlation length of 35 ± 1 Å (the inverse of the half width at half maximum). At energies of 25–30 meV [Fig. 2(e)] the line shape is also centered on the magnetic wave vector, but it now contains two peaks which can just be resolved [another example can be seen in Fig. 5(g)]. The fitted width of these peaks corresponds to a correlation length of 24 ± 2 Å. As the energy increases, the right hand of the two peaks grows while the left-hand peak diminishes. This asymmetry is not instrumental in origin, e.g., a resolution or background effect, because we observe it in scans measured under very different conditions on different spectrometers. Above $E\approx40$ meV the left-hand peak has virtually no intensity, as can be seen in Fig. 2(f).

Figure 3 shows the dispersion of the spin excitations obtained from Gaussian fits to the peaks observed in cuts such as those displayed in Figs. 2(d)–2(f). The points in Fig. 3 are the fitted peak centers corrected for the effect of the nonzero width of the cut perpendicular to the cut direction. For this purpose the scattering was taken to be a circle centered on the magnetic wave vector. Within the experimental limits of our data the dispersion was found to be the same in orthogonal cut directions.

In constructing the dispersion curve we had to take care to avoid confusing the scattering from magnetic excitations and phonons, especially in the energy range 10–40 meV, where the phonon scattering is particularly strong. One check we made was to compare data obtained at 300 K with that obtained at 10 K. Phonon scattering increases in strength with temperature, whereas magnetic scattering decreases in strength above the magnetic ordering temperature.

At energies above 50 meV we observed a broad ring of scattering centered on (0.5, 0.5). This is illustrated in Fig. 4, which shows (a) a constant-energy slice averaged over the energy range 51–54 meV and (b) a cut through this data along the line $(\xi,1-\xi)$ direction. This mode disperses away from (0.5, 0.5) with increasing energy, but was too weak to measure above 56 meV. This scattering was found to be slightly weaker at 300 than at 10 K, which suggests a mag-

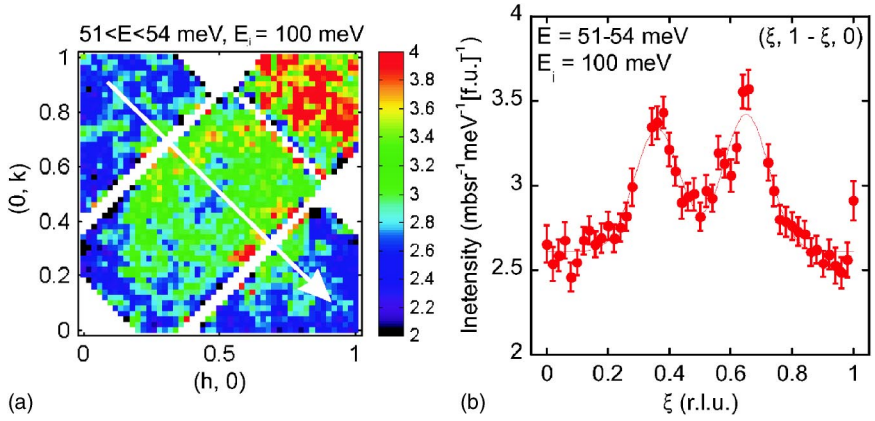

FIG. 4. (Color online) Neutron-scattering measurements from $La_{3/2}Sr_{1/2}NiO_4$ measured on MAPS at $T=10$ K. (a) Constant-energy slice through the data showing the intensity distribution in the (h,k) plane in the energy range 51–54 meV. The slice reveals weak diffuse scattering symmetrically distributed around (0.5, 0.5). Data from four equivalent Brillouin zones have been averaged to improve the statistics. (b) Cut through the 51–54 meV slice along the path indicated by the arrow in (a).

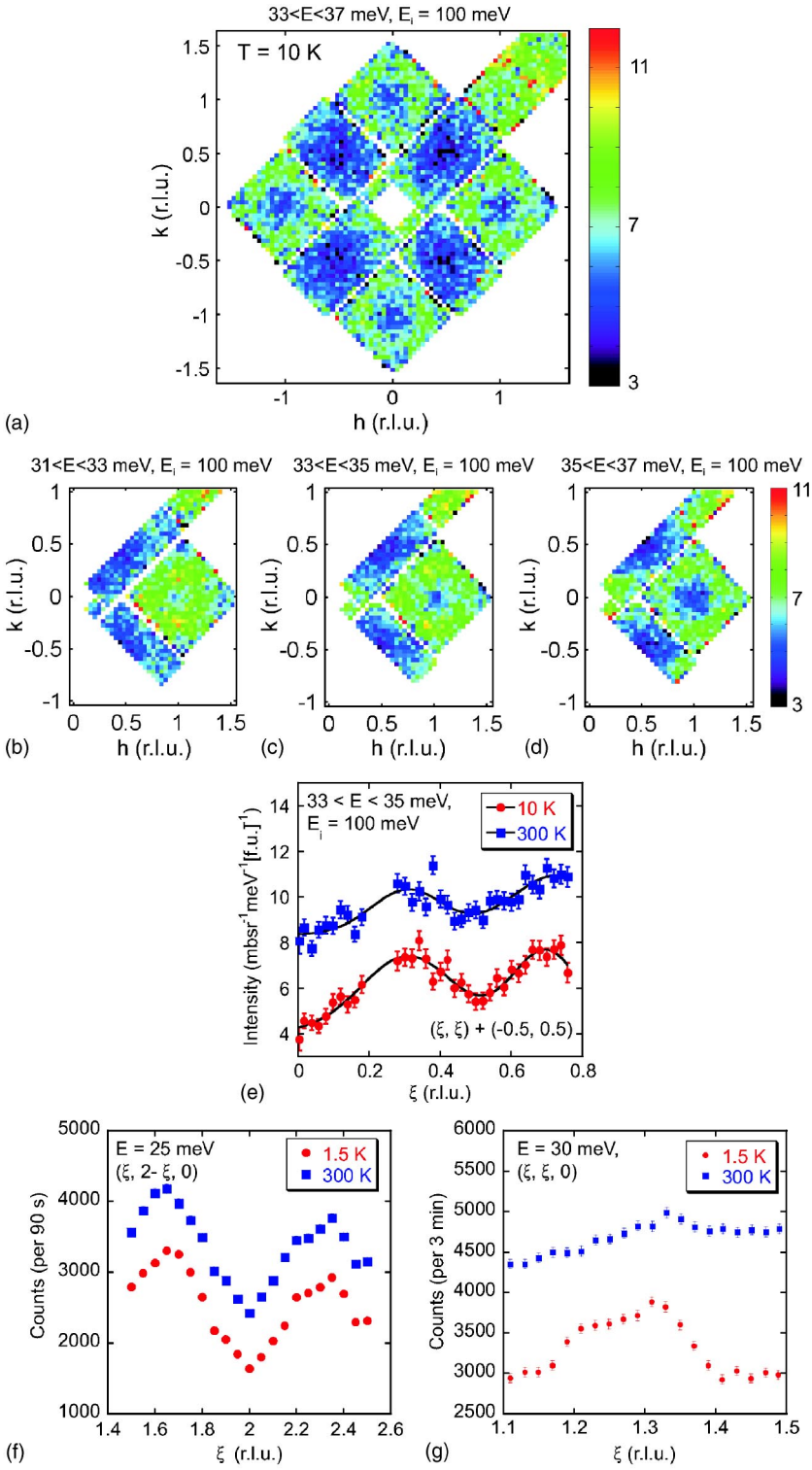

FIG. 5. (Color online) Excitations from $La_{3/2}Sr_{1/2}NiO_4$. (a) Distribution of scattering intensity in the (h,k) plane measured on MAPS at $T=10$ K. The scattering has been averaged over the energy range $E=33-37$ meV. (b)–(d) Slices through the scattering intensity measured at $T=10$ K in the (h,k) plane averaged over the energy ranges (b) 31–33 meV, (c) 33–35 meV, (d) 35–37 meV. The data in the MAPS detector have been folded to take advantage of the symmetry of the scattering. (e) Cuts through the data shown in (c) along a line parallel to the (h,h) direction passing through (1, 0). The data at $T=10$ and 300 K, have been offset by 5 units. The lines in (e) are the result of fitting the points with two Gaussian functions on a sloping background. (f) Scans of the scattering observed at $E=25$ meV for $T=1.5$ and 300 K measured on IN8. (g) A scan through the spin wave dispersion at $E=30$ meV for $T=1.5$ K and 300 K measured on IN8. The 300 K data in (f) and (g) have been offset by the addition of 1000 counts.

netic origin for it. We have added the peak positions of this scattering to the dispersion curve in Fig. 3.

In the energy range 31–39 meV we observed an interesting scattering feature separate from the main spin wave scattering. Figure 5(a) shows the distribution of intensity measured on MAPS for energies averaged over the range 33–37 meV covering a large area of reciprocal space. This intensity map displays strong diffuse scattering rings centered on the reciprocal lattice zone centers (h,k), where h and k are integers. Figures 5(b)–5(d) present constant-energy slices through this scattering centred on energies of 32, 34, and 36 meV. In these slices the symmetry-equivalent data have been folded into one quadrant to improve the statistics. The intensity is seen to disperse away from the (1, 0) point. In these measurements the out-of-plane component of the scattering vector varies from $l=2.5$ to 4. A search was made with the IN8 spectrometer of other Brillouin zones in the $(h,k,0)$ reciprocal lattice plane. This survey confirmed the

results found on MAPS, showing that the scattering was not restricted to a particular out-of-plane component of the scattering vector.

To assess whether or not this scattering is magnetic we performed measurements as a function of temperature. Cuts through the MAPS data at 10 and 300 K are shown in Fig. 5(e). These data show the scattering to decrease slightly with temperature, being approximately 45±12% stronger at 10 K than at 300 K. We also observed similar scattering in the range 25–30 meV. Figure 5(f) shows **Q** scans through the point (2, 0, 0) at an energy of 25 meV for temperatures of 1.5 and 300 K, measured on IN8. The scattering here appears to be temperature independent. To understand these temperature effects we need to take into account that this diffuse scattering ring overlaps the magnetic ordering wave vectors, so will contain some spin-wave scattering. The spin-wave scattering itself will, of course, be temperature dependent. To illustrate this we show in Fig. 5(g) scans through the spin-wave scattering associated with the magnetic wave vector $(1.5,1.5)-(\epsilon/2,\epsilon/2)$ measured at a slightly higher energy ($E=30$ meV) on IN8 at $T=1.5$ and 300 K. The amplitude of the spin-wave scattering clearly decreases with temperature. From this loss of intensity we can infer the temperature dependence of the remaining component of the scattering in Figs. 5(a)–5(f). Our analysis indicates that at $E\sim 35$ meV the non-spin-wave component of the diffuse scattering ring presented in Figs. 5(a)–5(d) decreases in intensity with temperature, whereas at $E=25$ meV [Fig. 5(f)] it increases with temperature. This leads us to conclude that the diffuse scattering around the Brillouin zone centers shown in Figs. 5(a)–5(d) is most likely magnetic in origin.

Further support for this conclusion was provided by examining data we have collected on crystals of $La_{2-x}Sr_xNiO_4$ with $x=1/3$ and 0.275 under similar condition during a separate experiment on MAPS.[17] Constant-energy slices for $x=1/3$ and 0.275 in the energy range 31–39 meV do not show any diffuse scattering rings similar to those shown in Figs. 5(a)–5(d), so this feature seems to be specific to $x=1/2$. This makes it highly unlikely that this scattering comes from phonons intrinsic to the host lattice of $La_{2-x}Sr_xNiO_4$.

For energies below 30 meV we performed additional measurements with polarized neutrons. In this energy range there is strong scattering from phonons, and polarized neutrons were necessary to provide an unambiguous separation of the magnetic and nonmagnetic scattering. We were particularly interested in studying the magnetic scattering as a function of energy because earlier measurements on $La_{2-x}Sr_xNiO_4$ compositions with $x=0.275$, 0.33, and 0.37 had revealed unexpected structure in the energy spectrum.[11,18] For these measurements the neutron polarization **P** was aligned parallel to the scattering vector **Q** so that the spin-flip (SF) channel would contain purely magnetic scattering.

The most interesting finding is reproduced in Fig. 6, which shows energy scans measured in the SF channel on samples with compositions $x=1/3$ and $x=1/2$ at their respective magnetic ordering wave vectors. The $x=1/3$ data contains two peaks, one centered on 7 meV and the other on 26 meV. The $x=1/2$ data contains a single peak at 5 meV.

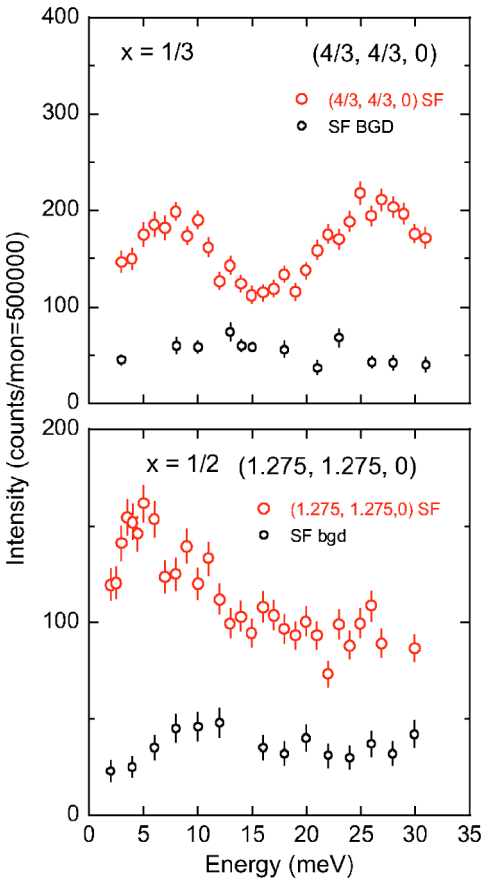

FIG. 6. (Color online) Polarized-neutron scattering from charge-ordered $La_{2-x}Sr_xNiO_4$ with $x=1/3$ and $1/2$. The plots show energy scans performed at the magnetic ordering wave vector appropriate to each composition. The spin-flip (SF) scattering was measured with $\mathbf{P}\|\mathbf{Q}$, and the SF background was estimated from scans centered away from the magnetic ordering wave vector. The measurements were made at 10 K for $x=1/2$ and 13.5 K for $x=1/3$.

The lower energy peaks were shown to be gaps due to spin anisotropy.[11,18] Below these gaps the out-of-plane spin fluctuations are quenched. The origin of the higher-energy peak in the $x=1/3$ data, which was first discussed in Ref. 11 and which was also found in similar data from crystals with $x=0.275$ and $x=0.37$,[18] remains a mystery. Of all the compositions studied, the one with $x=1/3$ exhibits this feature most strongly. The absence of a corresponding peak in the $x=1/2$ data seems to suggest that this peak is a property of compounds with static stripe order with a periodicity of ~ 3 lattice spacings. The monotonic decrease in intensity above 5 meV in the $x=1/2$ data is qualitatively consistent with the expected $1/E$ dependence of the cross section for scattering from antiferromagnetic spin waves.

Finally, we describe a feature observed in the scattering from $La_{3/2}Sr_{1/2}NiO_4$ at low energies. Figure 7(a) is a map of the intensity measured on IN8 covering part of the $(h,k,0)$ plane in reciprocal space. The map was constructed from a series of scans performed parallel to $(h,h,0)$ at an energy of 3 meV and a temperature of 2 K. Strong scattering can be seen centered on the magnetic ordering wave vectors, but additional weak diffuse scattering can also be seen centered

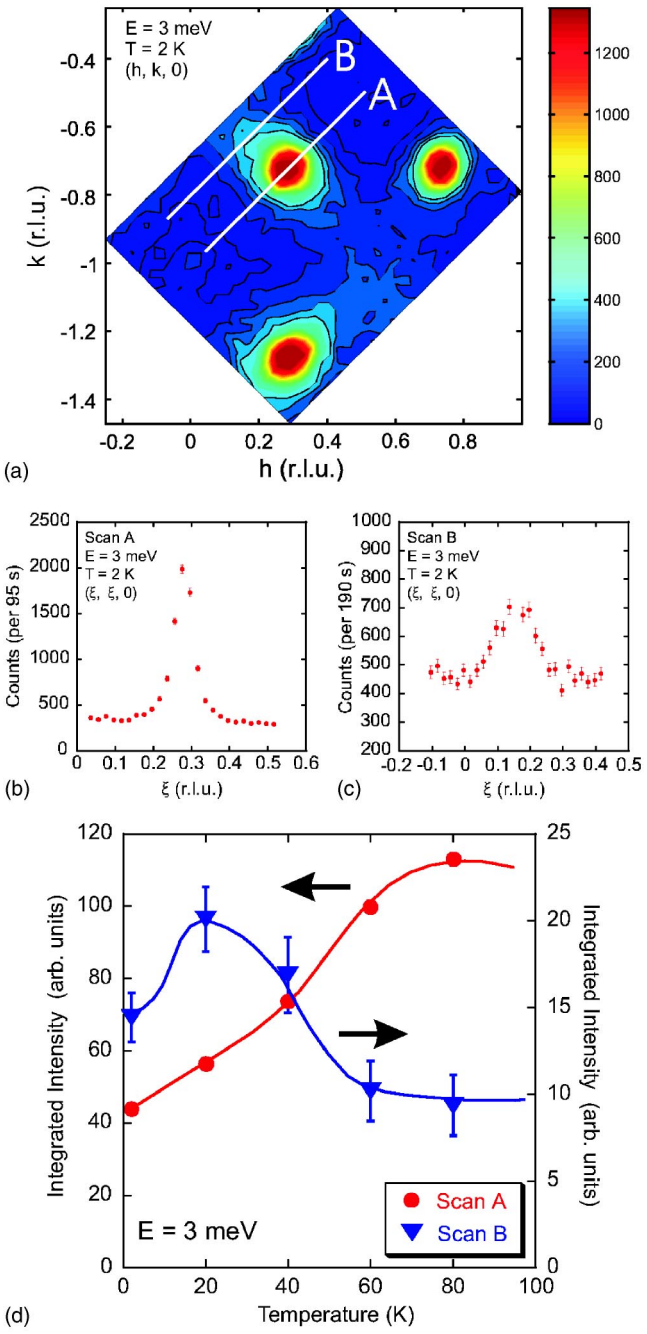

FIG. 7. (Color online) Low-energy scattering from $La_{3/2}Sr_{1/2}NiO_4$ measured on IN8 at an energy of 3 meV and a temperature of 2 K. (a) Map of the scattering intensity in the $(h,k,0)$ reciprocal lattice plane. (b) and (c) Cuts along the lines marked A and B in (a). (d) Temperature dependence of the integrated intensity of the peaks shown in (b) and (c). The lines are guides to the eye.

on these same positions. This diffuse scattering is slightly elongated in the diagonal directions, parallel to the discommensuration lines in the distorted checkerboard structure. There was no observable elastic diffuse scattering, so this feature represents a short-range dynamic magnetic correlation. We were able to follow the diffuse inelastic scattering up in energy to ~10 meV.

In Figs. 7(b) and 7(c) are shown scans through the spin-wave scattering and the diffuse scattering made along the lines marked A and B, respectively, in Fig. 7(a). Figure 7(d) displays the temperature dependence of the integrated intensity of the peaks in these two scans. The intensity for scan A is seen to increase with increasing temperature. This is due partly to thermal population of the spin waves, and partly to the reorientation of the ordered moment of the Ni^{2+} spins that takes place at 57 K.[8] Scan B, on the other hand, shows an initial increase in intensity on warming which peaks at around 20 K before decreasing at higher temperatures. This decrease suggests that the diffuse scattering is magnetic in origin, and the striking difference in temperature dependence between the spin-wave scattering and the diffuse scattering strongly indicates that they arise from two different magnetic components in the system.

IV. DISCUSSION

Let us first summarize the key observations, and then provide some quantitative analysis. From the various neutron-scattering measurements we have performed on spin- and charge-ordered $La_{3/2}Sr_{1/2}NiO_4$ we have been able to identify four distinct features: (1) dispersive spin excitation associated with the magnetic ordering wave vector, (2) low-energy diffuse spin dynamics also associated with the magnetic ordering wave vector but with a distinct temperature dependence, (3) a probable magnetic mode dispersing from (0.5, 0.5) at energies in the range 50–56 meV, and (4) a probable magnetic mode dispersing from (h,k) type positions in the energy range 31–39 meV. All these features are relatively broad in wave vector, and therefore arise from dynamic correlations that are short range in nature.

An obvious starting point for any analysis of the magnetic excitations in $La_{3/2}Sr_{1/2}NiO_4$ is the ideal checkerboard spin-charge-ordering pattern shown in Fig. 1(a). As far as the spins are concerned, this is a simple two-sublattice antiferromagnet built from $S=1$ spins on the Ni^{2+} sites. Spins attached to the Ni^{3+} sites are ignored for the time being. Following our previous work on stripe-ordered $La_{5/3}Sr_{1/3}NiO_4$,[11] we adopt a spin Hamiltonian of the form

$$H = J' \sum_{\langle i,j \rangle} \mathbf{S}_i \cdot \mathbf{S}_j + K_c \sum_i (\mathbf{S}_i^z)^2, \qquad (1)$$

where the first summation describes the exchange interactions between pairs of Ni^{2+} spins in linear Ni^{2+}-O-Ni^{3+}-O-Ni^{2+}bonds, and the second summation describes the small, *XY*-like, single-ion anisotropy. Here, as in Ref. 11, J' is defined as the exchange energy per spin (multiply by 2 to obtain the exchange energy per bond). We neglect the diagonal exchange couplings between Ni^{2+} sites which are needed to stabilize the spin arrangement but are assumed to be small relative to J'. In effect, therefore, the system is treated as two uncoupled square-lattice antiferromagnets with lattice parameter $2a$.

The magnon dispersion derived from Eq. (1) by standard linear spin-wave theory is given by

$$E(\mathbf{Q}) = 8J'S\{(1 + K_c/8J')^2 - [\gamma(\mathbf{Q}) \pm K_c/8J']^2\}^{1/2}, \quad (2)$$

where

$$\gamma(\mathbf{Q}) = \frac{1}{2}[\cos(2Q_x a) + \cos(2Q_y a)]. \quad (3)$$

The splitting of the two branches of the dispersion curve is such that at the magnetic zone center one mode is gapped and the other is not. The size of the gap is $4S(2J'K_c)^{1/2}$. When $K_c \ll J'$ the maximum energy of the dispersion curve is approximately $8J'S$.

In Fig. 3 we have plotted the spin wave dispersion along the (ξ,ξ) direction calculated from Eq. (2) with $S=1$, $J'=5.8$ meV, and $K_c=0.05$ meV. These parameters were chosen to match the observed maximum spin wave energy ($\sim$45 meV) and anisotropy gap ($\sim$3 meV). The spin-wave dispersion curve is seen to provide a reasonable description of the experimental data, apart from the obvious shift from the observed incommensurate wave vector (0.275, 0.275) to the ideal checkerboard wave vector of (0.25, 0.25). There is no detectable scattering from spin-wave modes on the dispersion curve near $\xi=0$ and $\xi=0.5$ because the antiferromagnetic structure factor is small in the magnetic Brillouin zones centered on (0, 0) and (0.5, 0.5).

From this analysis we can give a rough estimate of the exchange and anisotropy parameters for $La_{3/2}Sr_{1/2}NiO_4$. After consideration of the experimental errors, these are $J'=5.8\pm0.5$ meV and $K_c=0.05\pm0.02$ meV. It is interesting to compare these values with those derived from similar spin-wave analysis performed on other $La_{2-x}Sr_xNiO_4$ compositions. For $x=1/3$ the exchange parameters were found to be $J=15\pm1.5$ meV, $J'=7.5\pm1.5$ meV, and $K_c=0.07\pm0.01$ meV,[11] where J is the exchange interaction between Ni^{2+} spins on nearest-neighbor lattice sites. For undoped La_2NiO_4 the results were $J=15.5$ meV and $K_c=0.52$ meV.[19] This comparison shows that J' and K_c are similar for $x=1/3$ and $x=1/2$, but that K_c is very much larger in undoped La_2NiO_4. An explanation for why the single-ion anisotropy reduces so dramatically with doping is so far lacking.

We now discuss some of the obvious shortcomings of the model. We have already mentioned that the magnetic ordering wave vector in $La_{3/2}Sr_{1/2}NiO_4$ is $\mathbf{q}_m=(0.275,0.275)$ not (0.25, 0.25). Other problems are (1) the spin-wave scattering intensity above $\sim$25 meV becomes progressively more asymmetric about $\mathbf{q}_m$ with increasing energy, i.e., stronger on the side nearest to (0.5, 0.5)—see Figs. 2(e) and 2(f), and Fig. 5(g). This asymmetry disagrees with the spin-wave theory for the model described above, which predicts a symmetric scattering intensity about the magnetic zone center. (2) The extra scattering intensity observed around (0.5, 0.5) above 50 meV, and around (1,0) and equivalent positions in the energy range 31–39 meV suggest extra magnetic modes not present for a checkerboard ordering. (3) The spin-wave scattering is very broad, implying that the spin waves propagate only a few lattice spacings before being scattered or decaying into another excitation channel. (4) The source of the low-energy diffuse scattering needs to be identified.

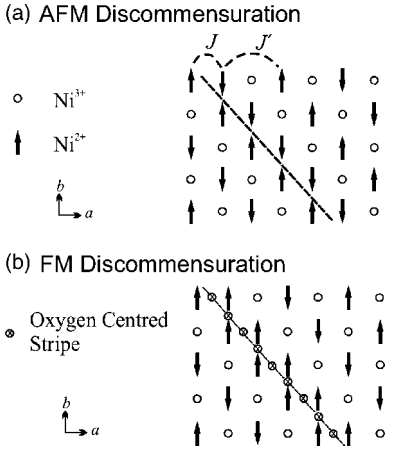

FIG. 8. (Color online) Two types of discommensuration that could exist in $La_{3/2}Sr_{1/2}NiO_4$ (Ref. 7). The spins on nearest-neighbor Ni sites have (a) antiparallel and (b) parallel alignment, respectively, in the discommensuration (indicated by a dashed line). Circles and arrows denote holes and $S=1$ spins, respectively, on the Ni sites. The encircled crosses in (b) denote the positions of an oxygen-centered charge stripe. The exchange interactions J and J' indicated in (a) couple spins on Ni^{2+} ions either on neighboring Ni sites (J) or on next-nearest-neighbor Ni sites separated by a Ni^{3+} ion (J').

To explain these features unequivocally we need a complete description of the static ordering, which we do not have. However, the idea that the static incommensurate order in $La_{3/2}Sr_{1/2}NiO_4$ can be understood in terms of an ideal checkerboard pattern broken up periodically by discommensurations is physically appealing,[7] and might provide some clues as to the origin of the various features in the spin excitation spectrum.

The two simplest types of discommensuration in the checkerboard pattern are illustrated in Fig. 8. The first [Fig. 8(a)] has a line of nearest-neighbor antiparallel spin pairs coupled by a superexchange interaction J expected to be close to 15 meV as found in the $x=0$ and $x=1/3$ compounds. Around the discommensuration the local hole density is below average. The second [Fig. 8(b)] has a line of holes on oxygen sites, which increases the local hole density and forces parallel alignment on neighboring Ni spins through the double exchange mechanism. We will refer to these as antiferromagnetic (AFM) and ferromagnetic (FM) discommensurations. More complex discommensurations involving a greater degree of perturbation of the ideal checkerboard pattern are also possible.

Discommensurations provide a mechanism for producing an incommensurate spin-density-wave modulation of the checkerboard pattern, as discussed earlier. At low energies, the magnon dispersion is expected to be similar to that of the ideal checkerboard antiferromagnetic ordering, except that the magnon dispersion is shifted away from (0.25, 0.25) to the incommensurate wave vector, as observed.

Let us focus, however, on the specific structure of the discommensurations themselves, which is expected to influence the spin-excitation spectrum at higher energies. The AFM discommensuration can be regarded as a zig-zag chain

with AFM intrachain exchange J coupled to the checkerboard AFM background. The latter has exchange J', and $J \approx 2J'$. Above the maximum energy of the spin-wave dispersion ($\sim$45 meV) we might expect to observe spin excitations characteristic of an AFM zig-zag chain. Because there will be discommensurations running along both diagonals the scattering will take the form of a square of scattering dispersing away from (0.5, 0.5) type positions, where the structure factor of the AFM zig-zag chain is largest. This could explain the observed "ring" of scattering apparently dispersing from (0.5, 0.5) at energies above 50 meV. At lower energies the spin excitations will have mixed checkerboard and zig-zag chain character, and this could explain why the spin-wave scattering becomes stronger on the side nearest to (0.5, 0.5).

Similarly, FM discommensurations resemble FM zig-zag chains. Spin excitations with FM zig-zag chain character are expected to be observable near to the structural zone centers. The strength of the intrachain double exchange is not known, but this effect could account for the mode dispersing from (h,k) type positions observed in the energy range 31–39 meV.

Discommensurations could also be responsible for the substantial widths of the spin-wave modes. In a region of commensurate checkerboard order a spin wave can propagate freely, but when it encounters a discommensuration the uniformity of the magnetic order is interrupted sharply, which could scatter the spin wave. In this case, the correlation length of the spin-wave peaks should correspond roughly to the average spacing between discommensurations. Earlier we found the correlation length to be 24 ± 2 Å for energies in the range 25–30 meV, which corresponds to approximately $9a/\sqrt{2}$, i.e., nine Ni positions when projected along the diagonal of the square lattice, which is the distance between discommensurations according to the model proposed by Kajimoto *et al.*[7] Further support for the broadening mechanism proposed here can be found from a comparison of the widths of spin-wave peaks observed in neutron-scattering measurements of $La_{2-x}Sr_xNiO_4$ with $x=0.275$ and $x=1/3$.[9] The $x=1/3$ spin-wave peaks show no measurable broadening, whereas the $x=0.275$ peaks are broadened. This is consistent with our broadening mechanism since the stripe order of $x=1/3$ is commensurate and without discommensurations, whereas that of $x=0.275$ is incommensurate and does have discommensurations.

This leaves us one remaining feature of the spin-excitation spectrum to consider, namely, the low-energy diffuse scattering distributed around the magnetic ordering wave vectors, shown in Fig. 7. As mentioned earlier, this scattering has a different temperature dependence to the spin-wave scattering, and from this we can conclude that it arises from a different magnetic component to the ordered spins. Low-energy diffuse scattering was also observed in the spin-excitation spectrum of $La_{5/3}Sr_{1/3}NiO_4$.[12] In that case the diffuse scattering was almost one-dimensional and, similar to the present case, there was no static component.

We attributed the quasi-1D diffuse scattering from $La_{5/3}Sr_{1/3}NiO_4$ to dynamic AFM correlations among the $S=\frac{1}{2}$ spins attached to lines of Ni^{3+} holes in the charge stripes, and the origin of the diffuse scattering from $La_{3/2}Sr_{1/2}NiO_4$ is probably the same. Because the Ni^{3+} holes are arranged on a near-checkerboard pattern in $La_{3/2}Sr_{1/2}NiO_4$ the spin correlations among the Ni^{3+} sites are expected to be quasi-2D, consistent with the observed diffuse scattering. The slight elongation of the scattering distribution is consistent with the introduction of a stripelike texture into the checkerboard pattern by discommensurations. The width of the peak shown in Fig. 7(c) is roughly twice that of an equivalent cut through the diffuse scattering from $La_{5/3}Sr_{1/3}NiO_4$. This indicates that the correlations between the Ni^{3+} spins are weaker in $La_{3/2}Sr_{1/2}NiO_4$. The interpretation of the diffuse scattering in $La_{3/2}Sr_{1/2}NiO_4$ presented here implies that there exists an AFM coupling between the Ni^{3+} spins that generates short-range fluctuations towards a checkerboard ordering. The absence of static magnetic order on the Ni^{3+} sites could have implications for recent predictions of orbital ordering in $La_{3/2}Sr_{1/2}NiO_4$.[20]

Finally, it is worth comparing our results with those obtained on other checkerboard charge-ordered compounds. To our knowledge, the only other such compound whose spin-excitation spectrum has been measured in detail is $La_{3/2}Sr_{1/2}CoO_4$.[21] The spin-charge order is much closer to a perfect checkerboard pattern in the half-doped cobaltate than in the half-doped nickelate. The incommensurability observed at low temperatures for $La_{3/2}Sr_{1/2}CoO_4$ is $\epsilon=0.49$,[4] compared with $\epsilon=0.44$ for $La_{3/2}Sr_{1/2}NiO_4$. Recall that for a perfect checkerboard order $\epsilon=0.5$. The measured spin-excitation spectrum of $La_{3/2}Sr_{1/2}CoO_4$ exhibits a simple spin-wave dispersion extending up 16 meV, and a second mode at energies around 30 meV which is relatively flat.[21] The spin-wave dispersion does not exhibit any of the unusual features found in the case of $La_{3/2}Sr_{1/2}NiO_4$. This can be understood if, as argued above, the deviations from a simple spin-wave picture are due to discommensurations: the very small incommensurability of the cobaltate implies very few discommensurations are present. The absence of low-energy diffuse scattering from the cobaltate also makes sense if the Co^{3+} ions are in a nonmagnetic singlet ground state, as is believed to be the case.[4]

V. CONCLUSIONS

The spin-excitation spectrum of $La_{3/2}Sr_{1/2}NiO_4$ has been found to contain a number of interesting features. We have argued that the low-energy diffuse scattering, which resembles a similar signal previously observed in measurements on $La_{5/3}Sr_{1/3}NiO_4$, originates from antiferromagnetic correlations among spins attached to the Ni^{3+} ions. We have also argued that other strange features in the excitation spectrum of $La_{3/2}Sr_{1/2}NiO_4$, such as the probable magnetic modes of scattering dispersing from (0.5, 0.5) and (1, 0) type positions and the large intrinsic widths of the spin excitations, can be understood (at least at the level of hand waving) in terms of a discommensuration model. The main obstacle in the way of a more quantitative account of the spin excitation spectrum of $La_{3/2}Sr_{1/2}NiO_4$ is the lack of a detailed model for the ground-state order.

ACKNOWLEDGMENTS

We would like to thank L. M. Helme for help in calculating the linear spin-wave dispersion, and José Lorenzana for stimulating discussions. This work was supported in part by the Engineering and Physical Sciences Research Council of Great Britain.

*URL: http://xray.physics.ox.ac.uk/Boothroyd

[1] J. M. Tranquada, B. J. Sternlieb, J. D. Axe, Y. Nakamura, and S. Uchida, Nature (London) **375**, 561 (1995).

[2] C. H. Chen, S-W. Cheong, and A. S. Cooper, Phys. Rev. Lett. **71**, 2461 (1993).

[3] Y. Moritomo, Y. Tomioka, A. Asamitsu, Y. Tokura, and Y. Matsui, Phys. Rev. B **51**, R3297 (1995); B. J. Sternlieb, J. P. Hill, U. C. Wildgruber, G. M. Luke, B. Nachumi, Y. Moritomo, and Y. Tokura, Phys. Rev. Lett. **76**, 2169 (1996); Y. Murakami, H. Kawada, H. Kawata, M. Tanaka, T. Arima, Y. Moritomo, and Y. Tokura, *ibid.* **80**, 1932 (1998).

[4] I. A. Zaliznyak, J. P. Hill, J. M. Tranquada, R. Erwin, and Y. Moritomo, Phys. Rev. Lett. **85**, 4353 (2000).

[5] J. E. Hoffman, E. W. Hudson, K. M. Lang, V. Madhavan, H. Eisaki, S. Ucida, and J. C. Davis, Science **295**, 466 (2002).

[6] T. Hanaguri, C. Lupien, Y. Kohsaka, D.-H. Lee, M. Azuma, M. Takano, H. Takagi, and J. C. Davis, Nature (London) **430**, 1001 (2004).

[7] R. Kajimoto, K. Ishizaka, H. Yoshizawa, and Y. Tokura, Phys. Rev. B **67**, 014511 (2003).

[8] P. G. Freeman, A. T. Boothroyd, D. Prabhakaran, D. González, and M. Enderle, Phys. Rev. B **66**, 212405 (2002).

[9] A. T. Boothroyd, P. G. Freeman, D. Prabhakaran, H. Woo, K. Nakajima, J. M. Tranquada, K. Yamada, and C. D. Frost, J. Magn. Magn. Mater. **272–276**, 265 (2004).

[10] P. Bourges, Y. Sidis, M. Braden, K. Nakajima, and J. M. Tranquada, Phys. Rev. Lett. **90**, 147202 (2003).

[11] A. T. Boothroyd, D. Prabhakaran, P. G. Freeman, S. J. S. Lister, M. Enderle, A. Hiess, and J. Kulda, Phys. Rev. B **67**, 100407(R) (2003).

[12] A. T. Boothroyd, P. G. Freeman, D. Prabhakaran, A. Hiess, M. Enderle, J. Kulda, and F. Altorfer, Phys. Rev. Lett. **91**, 257201 (2003).

[13] H. Yoshizawa, T. Kakeshita, R. Kajimoto, T. Tanabe, T. Katsufuji, and Y. Tokura, Phys. Rev. B **61**, R854 (2000).

[14] In this work we describe the structural properties of $La_{2-x}Sr_xNiO_{4+\delta}$ with reference to a tetragonal unit cell with cell parameters $a \approx 3.8$ Å and $c \approx 12.7$ Å.

[15] D. Prabhakaran, P. Isla, and A. T. Boothroyd, J. Cryst. Growth **237**, 815 (2002).

[16] On a time-of-flight spectrometer with the incident neutron beam parallel to the c axis the out-of-plane wave vector component l varies with the excitation energy, and depends also on the incident neutron energy. The l values for the data shown in Fig. 2 are given in the figure caption. Although the magnetic excitation spectrum of $La_{2-x}Sr_xNiO_4$ is highly two dimensional, the scattering intensity does vary with l. The variation is smooth, and depends partly on the magnetic form factor and partly on the direction of **Q**, since neutrons scatter from spin fluctuations perpendicular to **Q**. The ordered moment in $La_{3/2}Sr_{1/2}NiO_4$ lies in the ab plane, so the scattering becomes less sensitive to magnetic fluctuations parallel to the c axis as l increases.

[17] H. Woo A. T. Boothroyd, K. Nakajima, T. G. Perring, C. D. Frost, P. G. Freeman, D. Prabhakaran, K. Yamada, and J. M. Tranquada (unpublished).

[18] A. T. Boothroyd, P. G. Freeman, D. Prabhakaran, M. Enderle, and J. Kulda, Physica B **345**, 1 (2004).

[19] K. Nakajima *et al.*, J. Phys. Soc. Jpn. **62**, 4438 (1993).

[20] T. Hotta and E. Dagotto, Phys. Rev. Lett. **92**, 227201 (2004).

[21] L. M. Helme, A. T. Boothroyd, D. Prabhakaran, F. R. Wondre, C. D. Frost, and J. Kulda, Physica B **350**, 273 (2004).